Hindawi
International Journal of Corrosion
Volume 2018, Article ID 5389829, 10 pages
https://doi.org/10.1155/2018/5389829

Research Article

Experimental Assessment of Rebar Corrosion in Concrete Slab Using Ground Penetrating Radar (GPR)

Ahmad Zaki,[1] **Megat Azmi Megat Johari**,[2]
Wan Muhd Aminuddin Wan Hussin,[2] **and Yessi Jusman**[3]

[1]*Department of Civil Engineering, Universitas Abdurrab, Pekanbaru, 28291 Riau, Indonesia*
[2]*School of Civil Engineering, Engineering Campus, Universiti Sains Malaysia, Nibong Tebal, 14300 Penang, Malaysia*
[3]*Department of Electrical Engineering, Faculty of Engineering, Universitas Muhammadiyah Yogyakarta Kasihan, Bantul 55183, Yogyakarta, Indonesia*

Correspondence should be addressed to Ahmad Zaki; ahmad.zaki@univrab.ac.id

Received 29 January 2018; Revised 9 July 2018; Accepted 17 July 2018; Published 21 November 2018

Academic Editor: Michael I. Ojovan

Corrosion of steel reinforcement is a major cause of structural damage that requires repair or replacement. Early detection of steel corrosion can limit the extent of necessary repairs or replacements and costs associated with the rehabilitation works. The ground penetrating radar (GPR) method has been found to be a useful method for evaluating reinforcement corrosion in existing concrete structures. In this paper, GPR was utilized to assess corrosion of steel reinforcement in a concrete slab. A technique for accelerating reinforcement bar corrosion using direct current (DC) power supply with 5% sodium chloride (NaCl) solution was used to induce corrosion to embedded reinforcement bars (rebars) in this concrete slab. A 2 GHz GPR was used to assess the corrosion of the rebars. The analysis of the results of the GPR data obtained shows that corrosion of the rebars could be effectively localized and assessed.

1. Introduction

Corrosion of steel reinforcement is a worldwide problem of concrete structures [1]. Corrosion has been recognized as a major deterioration phenomenon which leads to the structural concrete degradation due to environmental actions [2]. Many reports have highlighted that all over the world concrete structures are damaged by corrosion and the costs associated with repair and maintenance required worldwide have exceeded billions of dollars [3]. Successful repair to concrete structures requires reliable information on the concrete structural conditions, including the cause of damage, degree of damage, and effect of damage on the actual structural behaviour.

Visual inspection of the whole structure to assess the condition of corrosion in concrete structures regarding reinforcement corrosion is a common regular inspection method but it is highly dependent on the expertise of the operator as unseen corrosion is not easily detected [2]. Meanwhile, the half-cell potential (HCP) technique is the most widely used nondestructive test to detect and localize rebar corrosion. The half-cell potential technique is based on electrochemical principles which provides information pertaining to the probability of reinforcement corrosion in concrete structures [2, 4]. On the other hand, ground penetrating radar (GPR), an alternative nondestructive testing (NDT) method, has become a valuable tool for inspection of concrete structures over the past few years [5]. GPR is capable of early detection of reinforcement corrosion in concrete structures [6–11]. Based on the capability of the GPR method to investigate corrosion, this paper proposes an assessment of rebar corrosion using GPR on a concrete slab with embedded corroded steel bars.

2. Literature Review

2.1. Ground Penetrating Radar (GPR). GPR, an electromagnetic (EM) investigative method, is mostly used in the reflection mode where a signal is emitted via an antenna into the structure under investigation. The reflected energy

caused by changes in material properties is recorded and analyzed [12, 13]. Development of GPR has evolved over the past 35 years. Early research related to GPR focused on the possibilities and applicability of GPR. The first application of GPR in 1904 was to detect metal objects [14]. The use of GPR for civil engineering applications commenced in the 1980s [15]. Cantor [16] developed the basis of analysis and interpretation techniques in these areas. Furthermore, Clemena [17] utilized GPR for testing of concrete structures. GPR is a possible method for periodic inspection and maintenance of concrete structures [18]. Generally, GPR technology may be employed for localization of reinforcing bars, localization of cracking, localization and assessment of voids, localization of honeycombed or cracking, corrosion detection, estimation of bar size, concrete mix proportions, and environmental conditions [10, 19–31].

The principles of nondestructive testing (NDT) by GPR involve the transmission of EM waves into a structure under investigation. The propagation of EM waves of GPR depends on the corresponding dielectric properties of the materials [32–34]. Permittivity in turn depends on the EM properties which are influenced by temperature, moisture content, salt content, pore structure, and pulse frequency [35]. Whenever EM waves encounter an interface of two media having different dielectric constants, part of the wave is reflected back to the receiving antenna. The amount of scattering depends upon the contrast in dielectric properties of the two media [36]. The values of the dielectric constant for a variety of materials range from 1 to 81 (1 = air, 81 = water) [35]. EM waves propagate through the medium and are reflected at interfaces of materials with different dielectric properties. The reflected waves are recorded by a receiving antenna. These received waves are then converted into a voltage wave, which is called a trace (*a*-scan), as shown in Figure 1. GPR systems generate rapid successions of traces, which are displayed as a so-called radargram (*b*-scan) by investigating a material along a line, as shown in Figure 2(a). The other waves are displayed as time slice (*c*-scan) by investigating a material along a grid pattern, as shown in Figure 2(b) [37].

2.2. Accelerated Corrosion Process. In practice, corrosion of steel reinforcement in concrete structures is a long-term process. It takes quite a real long time for the initiation and propagation of corrosion. For a research study, it is not easy to achieve different degrees (i.e., levels of mass loss) of corrosion within a short period of time. Therefore, various methods for accelerating reinforcement corrosion in a concrete structure have been used by several researchers [39]. In many studies the impressed current technique has been used to study the mechanical behaviour of corroded concrete structures [40], bond behaviour of corroded rebars [41], structural behaviour of corroded structural concrete elements [42, 43], and the performance of concrete structures [44]. The advantages of using this technique are that a high degree of corrosion can be obtained within a short period of time and the easy control of the desired degree of corrosion.

The anodic reaction releases electrons, while the cathodic reaction consumes electrons. Figure 3 shows schematically the process of corrosion of steel in concrete [3].

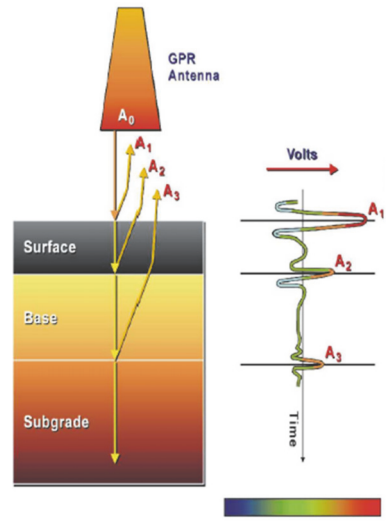

Figure 1: Single trace (*a*-scan) [38].

The anodic reaction depends on the pH of the electrolyte and the presence of anions. The anodic reaction for rebar corrosion is given by

$$\mathrm{Fe} \longrightarrow \mathrm{Fe}^{2+} + 2\mathrm{e}^{-} \quad \text{(for iron and steel)} \tag{1}$$

The impressed current technique is used for accelerating corrosion of steel reinforcement in concrete by applying direct current (DC) through an external power supply. The positive terminal of this DC power supply is connected to the rebar making it act as anode, while the negative terminal is connected to a counter electrode becoming a cathode. The counter electrode could be in the form of an internal bar [45], external mesh [46], or external plate [41, 47]. The concrete specimens should be partially immersed in sodium chloride (NaCl) solution in a suitable tank, where the NaCl solution is in direct contact with the bottom of the structure. Here, an NaCl solution functioned as the electrolyte. The amount of corrosion is related to the energy consumed, which is a function of voltage (V), amperage (A), and time interval. Usually, a constant voltage between the anode and cathode is applied through the DC power supply. The principle of the method is described in ASTM G1-03 [48] and ASTM G31-72 [49].

Corrosion is often reported in terms of weight loss per unit time or thickness loss per unit time and steel surface area. Corrosion rate is directly proportional to the measured electrical current density and total mass loss is related to the measured electrical current by Faraday's Law [50] as given by

$$\Delta \mathrm{m} = \frac{MIt}{zF} \tag{2}$$

where

Δm = mass of steel consumed (g);

M = atomic or molecular weight of metal (56 g for Fe);

I = current (amperes), t = time that current or potential is applied (seconds);

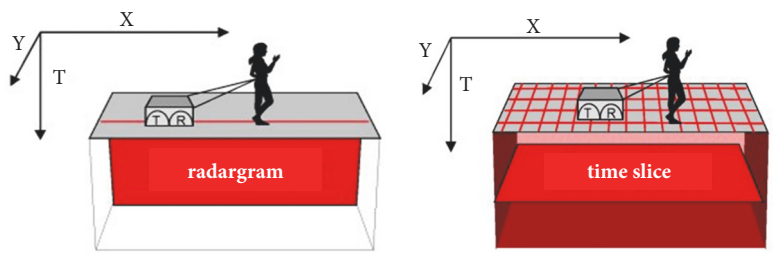

(a) (b)

Figure 2: (a) Radargram (b-scan) and (b) time slice (c-scan) [37].

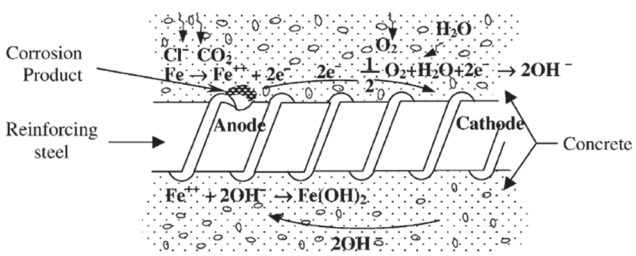

Figure 3: Process of corrosion of steel in concrete [3].

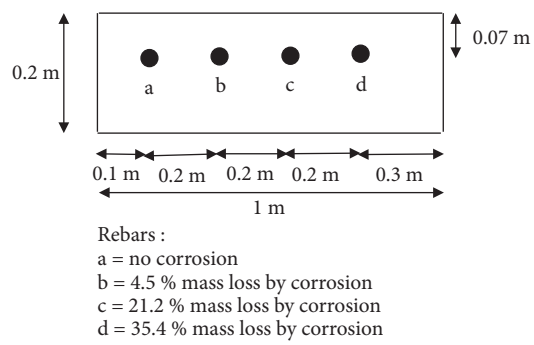

Figure 4: Schematic representation of concrete slab with rebars at different degrees of corrosion.

z = ionic charge or electrons transferred in the half-cell reaction (2 for Fe);

F = Faraday's constant (96,500 amp/sec).

Furthermore, the actual degree of corrosion or level of mass loss for the corroded steel specimens could be measured as the difference in mass of the bars before and after testing through equation [51]:

$$\mathrm{M}l = \frac{Mi - Mf}{Mi} \times 100 \quad (3)$$

where

$\mathrm{M}l$ = mass loss (%);

Mi = mass of noncorroded specimen weighed before the corrosion test (g)

Mf = mass of corroded specimen weighed after the corrosion test (g).

3. Materials and Methods

3.1. Specimens. Normal concrete with C30 grade was used in the experiment. The mix proportion includes 380 kg/m^3 Portland cement, 190 kg/m^3 water (w/c = 0.5), 780 kg/m^3 uncrushed sand (fine aggregate), and 1080 kg/m^3 crushed granite (coarse aggregate) with a maximum aggregate size of 20 mm. Average 28-day and 150-day compressive strengths are 44.43 MPa and 58.88 MPa, respectively. Type deformed steel reinforcement is selected for the rebars having a diameter of 20 mm. The exposed length of the rebars is 0.6 m.

A concrete slab was prepared having dimensions of length (l) = 1 m, width (w) = 0.5 m, and height (h) = 0.2 m. Figure 4 shows a schematic representation of this concrete slab. After 28 days of moist curing, a DC current was impressed on three embedded rebars (i.e., rebars b, c, and d) embedded in this concrete slab. Corrosion of the individual rebars was accelerated by varying the duration of the applied current in order to achieve the intended degree of corrosion. The positive terminal of a DC power supply was connected to a rebar as anode, while the negative terminal was connected to a cathode. Here, a copper plate was used as the external cathode completely submerged in an NaCl solution. The slab was partially immersed in a solution of 5% NaCl and 95% distilled water stored in a plastic tank. The NaCl solution was in direct contact with the bottom of the slab. A photo of the test setup is shown in Figure 5.

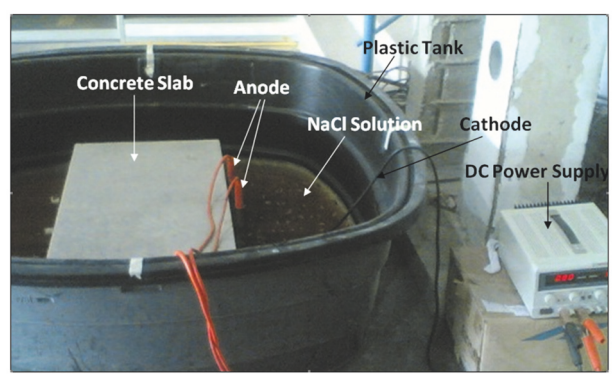

Figure 5: A photo of the impressed current technique.

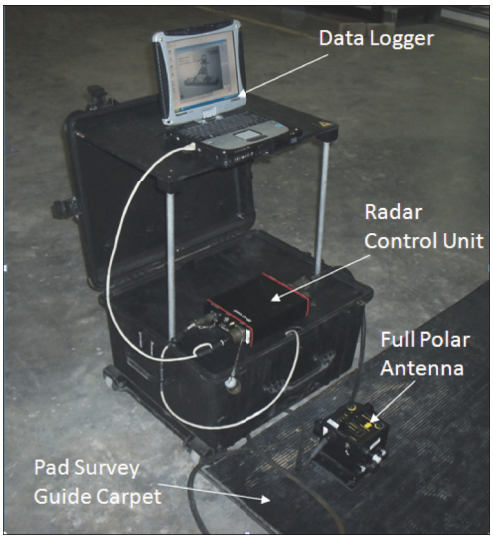

Figure 6: GPR ALADDIN SK2 kit.

Table 1: The duration of current applied for each rebar.

Rebar	Current applied (days)	Corrosion Degrees (%)	Current Density (mA/cm^2)
a	0	0.359	0
b	20.85	4.527	3.973
c	54.53	21.263	19.034
d	84.91	35.359	31.158

During the full duration of the test, a total anodic current of 0.4 A was applied to accelerate the corrosion process for a set of 3 rebars (rebar b-c-d). The process was continued until the different rebars were corroded to the required degree by varying the exposure times. The required duration of the applied current is calculated from the different degrees of corrosion. Faraday's law was applied to the accelerated technique. Firstly, the mass loss (Δm) was calculated using Faraday's law as illustrated in (2) [50]. Secondly, the corrosion levels of the rebars were based on the percentage of the difference between weight of initial and final mass using (2) [52]. Table 1 shows the duration of current applied for each of the 3 rebars.

3.2. GPR Acquisitions. The GPR equipment used in this research was manufactured by IDS (Ingegneria Dei Sistemi S.p.A) Pisa, Italy, as shown in Figure 6. The special full-polar high-frequency antenna (2 GHz) was combined with the patented Pad Survey Guide (PSG). In this work, the previously described reinforced concrete slab was scanned using the GPR equipment. The 2 GHz GPR antenna with two polarizations (transversal and longitudinal) was able to identify both types of scanned targets (shallow and deep) in just one scan.

The slab was scanned in line on a PSG carpet. A line of scan step on the PSG carpet was 0.78 cm, as shown in Figure 7(a). The PSG carpet held alternate upper and lower guides in order to make the slide perfectly fit and for the antenna to realize straight scans. Also, the slide held a special film on its external surface removing minimum friction during the drag of the antenna on the PSG, as shown in Figure 7(b). Finally, the PSG held on its edge a graduated horizontal pole with the indication of numbers and letters in a progressive sequence, in order to give the user a reference point at the beginning of the scan.

The scanned GPR results were stored in a computer completed by IDS in the GPR set. After obtaining the images from GPR, GRED software was used to obtain data images which were subsequently processed using image processing techniques. Data image could be presented as *a*-scan, *b*-scan, *c*-scan, and 3D images.

4. Results and Discussions

4.1. Corrosion Levels. The corrosion levels of the 4 rebars embedded in the concrete slab are presented as qualitative and quantitative results. The qualitative results are shown in Figure 9. It shows the postcorrosion slab after the completion of the corrosion process (rebars a = no corrosion, b = 4.5% mass loss, c = 21.2% mass loss, and d = 35.4% mass loss) based on the calculation of (3). There are cracks in the concrete cover above rebar c and rebar d. The concrete cover of rebar d shows a clear macrocrack along the full length of the rebar. This type of crack could affect the integrity of the concrete slab.

After that, the concrete slab was broken to retrieve the corroded rebars. The rebars were cleaned according to ASTM G1-2003 standard to remove all corrosion products [48]. The cleaned rebars with different degree of corrosion after cleaning are shown in Figure 10. Finally, the cleaned rebars were weighed to quantify the mass loss due to corrosion according to (3).

4.2. Assessing Rebar Corrosion Using GPR. Figure 11 shows the *a*-scan of line 25 before the accelerated corrosion process. The line is used as a reference because line 25 is in the middle of the rebar and also represents the condition of the rebars. Rebars a, b, c, and d are conditions of rebars which agree with information contained in Table 1. In Figures 11–14, S_d refers to the direct wave signal and S_r is the reflected wave signal from the rebar-concrete interface. There are no significant differences in the waves peak (i.e., direct wave and reflected wave) in terms of amplitude and travel time for all four rebars, which indicates that the rebars are in good condition (no corrosion). The waves are very important for reinforced concrete durability as it can provide information on concrete cover, i.e., the thickness and quality (presence of defects) of the concrete cover [53]. Information on the wave peaks is shown in Table 2.

Figure 12 shows the *a*-scan of the concrete slab at line 25 after the completion of the corrosion process of rebar b at the 21st day. Table 3 provides information on the quantification of the *a*-scan shown in Figure 12. The amplitude of direct wave and reflected wave peak was increased because the frequency was attenuated due to the accelerated corrosion [34, 53, 54]. The amplitudes of rebars b, c, and d were higher than that of rebar a. These conditions could be caused by the

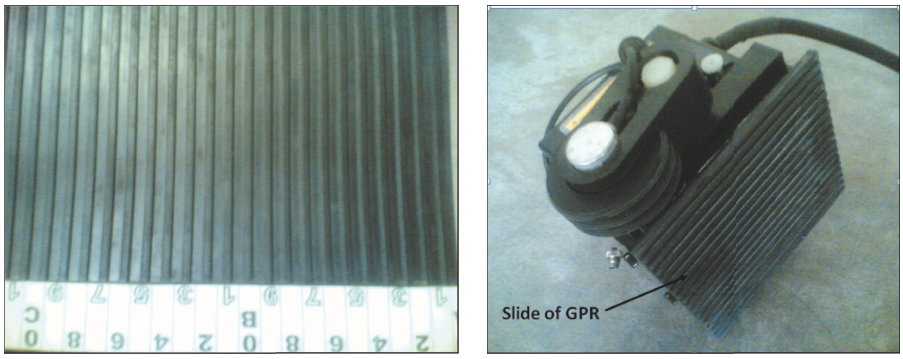

(a) (b)

Figure 7: Features: (a) PSG carpet with lines of scan and (b) slide of GPR.

Table 2: Quantification of *a*-scan derived from Figure 8.

	Rebar a		Rebar b		Rebar c		Rebar d	
	Amplitude Peak	Travel Time	Amplitude Peak	Travel Time	Amplitude Peak	Travel Time	Amplitude Peak	Travel Time
S_d	0.410	-0.19	0.41	-0.19	0.410	-0.19	0.410	-0.19
S_r	0.321	1.127	0.295	1.170	0.321	1.127	0.321	1.127

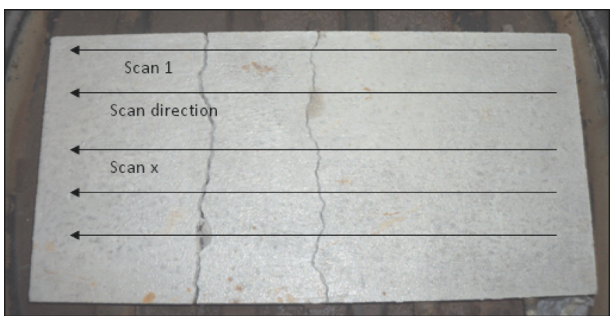

Figure 8: Scan direction of GPR.

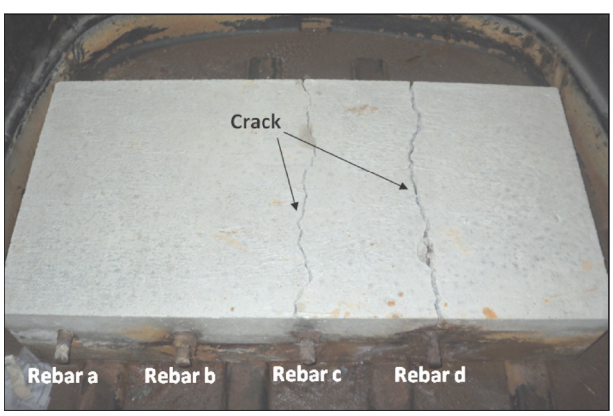

Figure 9: Concrete slab image after accelerated corrosion.

high content of chloride [35]. This may happen after cracking of the concrete cover, allowing faster ingress of chloride ions to the rebar; however prior to cracking hardly any chloride ions were present near the rebar. In this condition,

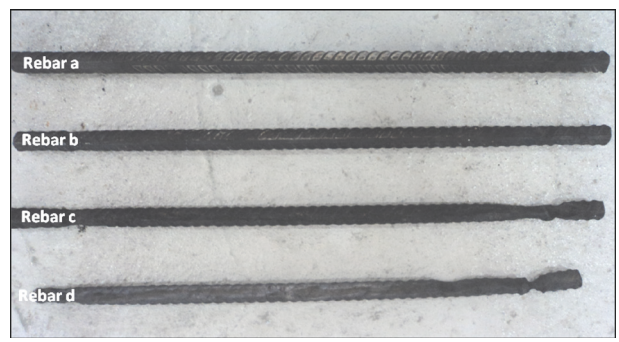

Figure 10: Corroded rebar of postcorrosion slab.

chloride ions were forced to accumulate around the rebar. The accumulation of ions attenuated and absorbed the reflected wave in both time and frequency.

Figure 13 shows the *a*-scan of the concrete slab at line 25 after the completion of the corrosion process of rebar c at the 55th day. The frequencies of the waves shift to lower regime due to the effect of the corrosion process. The reflected waves of rebar c have lower amplitude than that of rebars a, b, and d because it is likely that the corrosion process of rebar c was affected by the accumulation of chloride ions in the concrete cover zone of the rebar which is more than for the other rebars. The higher content of chloride ions retarded and absorbed the waves in both time and frequency [55, 56]. The quantification values of the waves are shown in Table 4.

Figure 14 shows the *a*-scan of the concrete slab at line 25 after the completion of the corrosion process of rebar d at the 85th day. The direct wave peaks of rebar d are higher than that of rebars a, b, and c. This condition may have happened due to the cracked concrete cover which affects rebar c. The presence of voids in the crack zones could have increased the amplitude

Table 3: Quantification of *a*-scan derived from Figure 9.

	Rebar a		Rebar b		Rebar c		Rebar d	
	Amplitude Peak	Travel Time	Amplitude Peak	Travel Time	Amplitude Peak	Travel Time	Amplitude Peak	Travel Time
S_d	0.410	0.310	0.505	0.311	0.466	0.307	0.570	0.311
S_r	0.357	1.059	0.460	1.062	0.416	1.062	0.407	1.050

Table 4: Quantification of *a*-scan derived from Figure 10.

	Rebar a		Rebar b		Rebar c		Rebar d	
	Amplitude Peak	Travel Time	Amplitude Peak	Travel Time	Amplitude Peak	Travel Time	Amplitude Peak	Travel Time
S_d	0.480	0.496	0.490	0.496	0.500	0.496	0.510	0.496
S_r	0.330	1.620	0.350	1.620	0.220	1.860	0.320	1.620

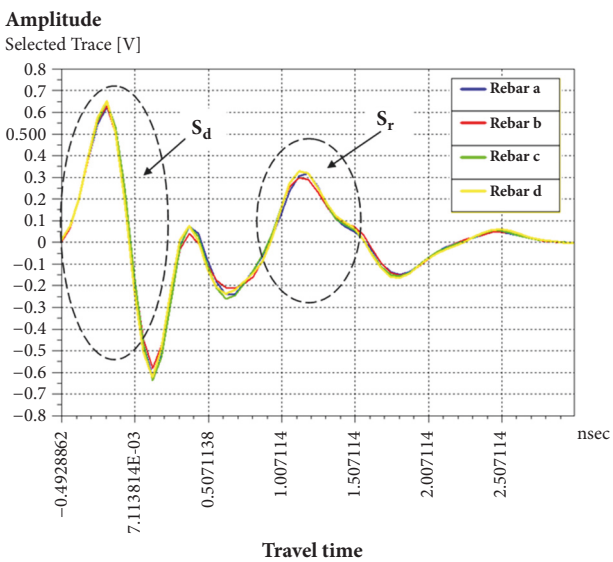

Figure 11: *a*-scan of the postcorrosion slab before accelerated corrosion.

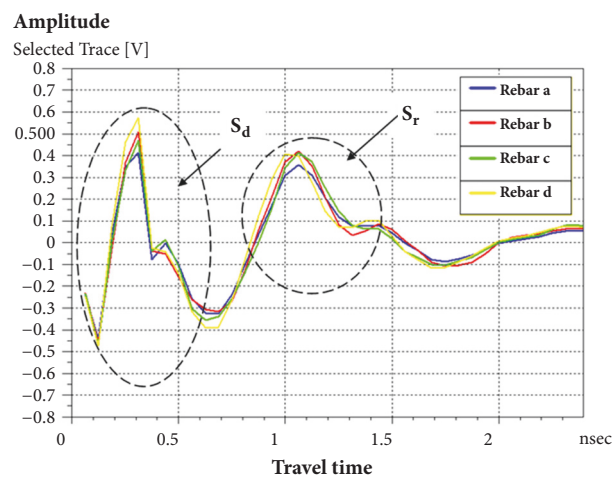

Figure 12: *a*-scan of the postcorrosion slab after accelerated corrosion of rebar b.

[34]. However, these phenomena did not happen for rebar d. As shown in Table 5, the higher content of moisture and chloride from the induced corrosion affects the amplitude of the reflected waves of GPR [35]. The moisture content and chloride content increase due to corrosion. Even though rebar a is supposed to have no corrosion, while rebar b was induced to have a low level of corrosion, rebars b and d show higher amplitudes (0.370 and 0.321, respectively) of reflected waves than rebar a (0.289). Rebar c has lower amplitude (0.213) and higher travel time (1.964 ns). It is likely that this has happened due to the high contents of chloride ions which cause an attenuating influence of waves and has stronger impact on rebar c than the other rebars [56, 57].

Figure 15 shows the *b*-scan of the rebars of the concrete slab in line 25. In Figure 15(a), there are no differences between the hyperbolic images and the respective depth of the rebars because the rebars are in good condition (no corrosion). In the case of Figure 15(b), the corrosion process has reduced the frequency signal of the waves whose effect is to reduce the hyperbolic image of the rebars. Meanwhile, in Figure 15(c), the image is fuzzy because of the formation and transport of corrosion products which cause an attenuating influence of waves and has strong impact to *b*-scan image [57]. The corrosion products of rebar c have diffused to a shallower cover depth, as shown in Figure 16(a). This may be due to the fact that the types of corrosion products when accelerating the corrosion process by an impressed current are different and less voluminous than the products formed under normal free corrosion conditions.

Finally, Figure 15(d) shows that the hyperbolic image of rebar c is significantly reduced due to corrosion. This can be explained by the *b*-scan image of rebar c which is fuzzier due to corrosion products that have diffused to closer proximity within the concrete surface [58], as shown in Figure 16(a). However, different phenomena could be observed in the *b*-scan image of rebar d. Rebar d is supposed to have a higher level of corrosion than rebar c, but the opposite condition is displayed from the *b*-scan. In theory, the image becomes fuzzy due to an increase of the corrosion level [59]. However, the image of rebar d shown is much clearer. The depth of the rebar image becomes shallower than the reference (rebar a). The probable explanation is that the energy of the wave was less attenuated due to corrosion products that diffused to a much shallower concrete cover [58], as shown in Figure 16(b). The amount of corrosion products of rebar d is more than that of rebar c; however the corrosion products of rebar d

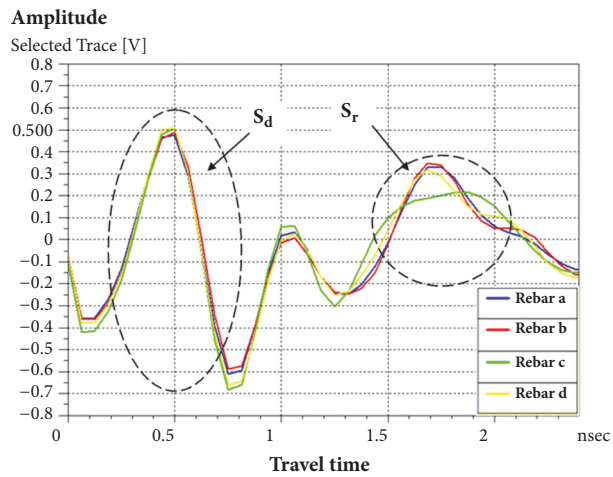

Figure 13: *a*-scan of the postcorrosion slab after accelerated corrosion of rebar c.

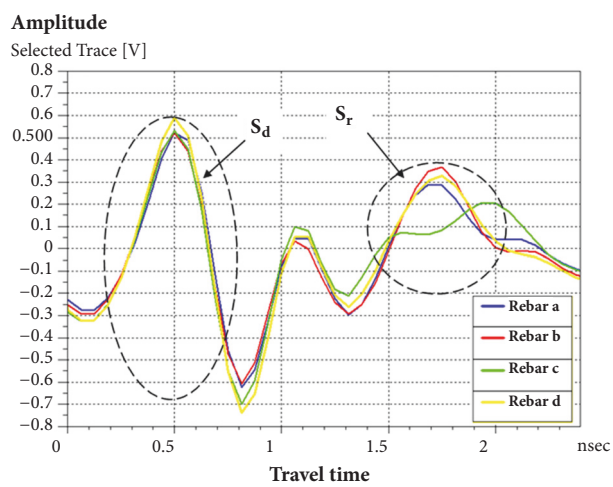

Figure 14: *a*-scan of the postcorrosion slab after accelerated corrosion of rebar d.

Table 5: Quantification of *a*-scan derived from Figure 11.

	Rebar a		Rebar b		Rebar c		Rebar d	
	Amplitude Peak	Travel Time	Amplitude Peak	Travel Time	Amplitude Peak	Travel Time	Amplitude Peak	Travel Time
S_d	0.528	0.502	0.528	0.502	0.528	0.502	0.590	0.502
S_r	0.289	1.750	0.370	1.750	0.213	1.964	0.321	1.750

(Figure 16(b)) have not diffused significantly to the concrete cover surface like the corrosion products of rebar c, as shown in Figure 16(a).

5. Conclusions

In this paper, it has been demonstrated that the presence of rebar corrosion in a concrete slab has been successfully assessed using GPR. The processes start with concrete slab fabrication followed by the results of imposed current technique and data collection by scanning a reinforced concrete slab using 2 GHz of the GPR. Several results can be obtained by using the GPR technique for assessing rebar corrosion in a concrete slab. The results are presented by the *a*-scan and the *b*-scan. The results show that rebar corrosion can be detected and identified at an early stage before visual damage or other signs of corrosion have appeared. The results of the *a*-scan, i.e., lower amplitude and larger travel times of the waves for corroded rebars, are probably due to increased chloride contents and presence of corrosion products. For the *b*-scan, the form of blurring and dimming of rebar image features shows a distinct indication of rebar corrosion due to chloride contents and corrosion product which have influenced the threshold level of image. Generally, the results of an a-scan can represent the condition of rebar corrosion damage. The impressed current results in uniform corrosion attack whereas in practice (real structures) chloride-induced corrosion normally will be characterised by strongly localised

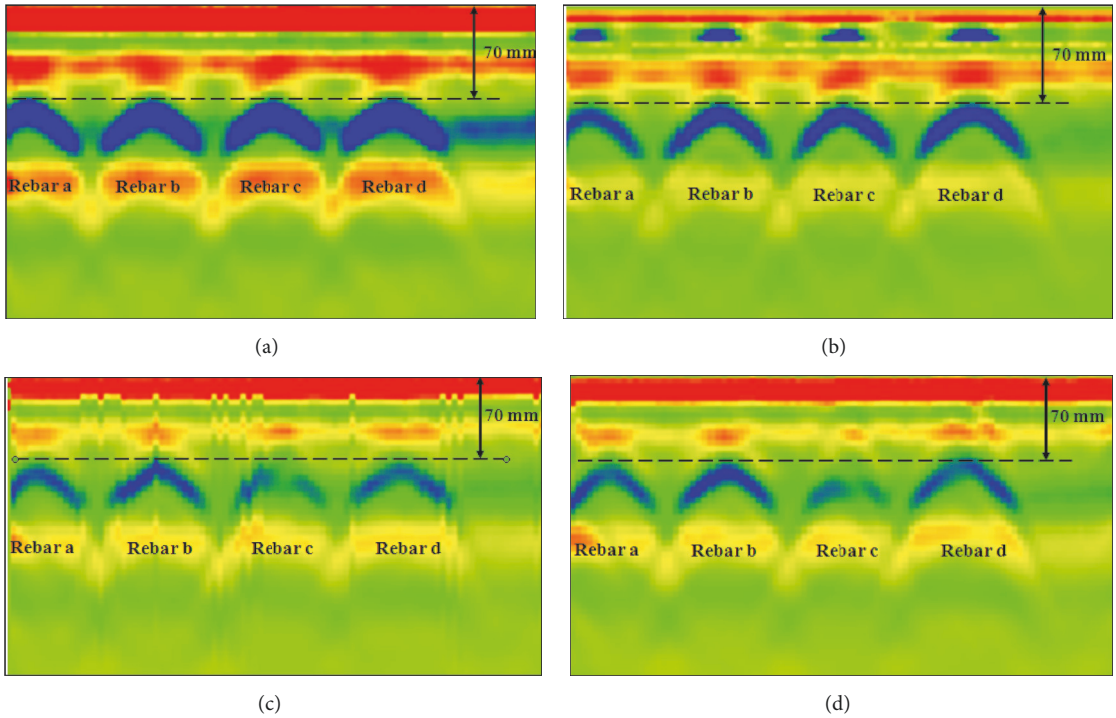

Figure 15: *b*-scan of the postcorrosion slab: (a) before accelerated corrosion, (b) after accelerated corrosion of rebar b, (c) after accelerated corrosion of rebar c, and (d) after accelerated corrosion of rebar d.

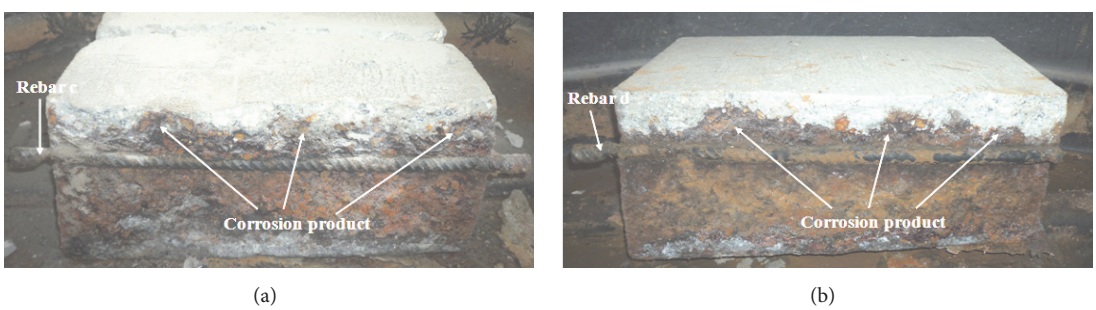

Figure 16: Cut sections of the postcorrosion slab: (a) rebar c and (b) rebar d.

corrosion attack. In summary the results obtained by GPR indicate that GPR can also effectively be used for assessment of localised corrosion damage of concrete slab in terms of chloride contents and corrosion product.

Data Availability

The authors state that all the data used in this study are included within the manuscript.

Conflicts of Interest

There are no conflicts of interest regarding the publication of this paper.

Acknowledgments

The authors would like to acknowledge the financial support provided by Universiti Sains Malaysia for providing RU-PGRS Grant Scheme entitled "Concrete Health Monitoring Using Non-Destructive Testing (NDT) Methods" and the financial support provided by Universitas Abdurrab, Pekanbaru, Indonesia.

References

[1] M. Badawi and K. Soudki, "Control of corrosion-induced damage in reinforced concrete beams using carbon fiber-reinforced polymer laminates," *Journal of Composites for Construction*, vol. 9, no. 2, pp. 195–201, 2005.

[2] B. Elsener, C. Andrade, J. Gulikers, R. Polder, and M. Raupach, "Hall-cell potential measurements—potential mapping on reinforced concrete structures," *Materials and Structures*, vol. 36, no. 261, pp. 461–471, 2003.

[3] S. Ahmad, "Reinforcement corrosion in concrete structures, its monitoring and service life prediction—a review," *Cement and Concrete Composites*, vol. 25, no. 4-5, pp. 459–471, 2003.

[4] A. Zaki, H. K. Chai, D. G. Aggelis, and N. Alver, "Non-destructive evaluation for corrosion monitoring in concrete: A review and capability of acoustic emission technique," *Sensors*, vol. 15, no. 8, pp. 19069–19101, 2015.

[5] H. Wiggenhauser, H. W. Reinhardt, D. O. Thompson, and D. E. Chimenti, "NDT in civil engineering: experience and results of the for 384 research group," in *Proceedings of the Review of Progress in Quantitative Nondestructive Evaluation*, vol. 29, pp. 47–54, Kingston, Rhode Island, RI, USA, 2010.

[6] G. R. Olhoeft, "Maximizing the information return from ground penetrating radar," *Journal of Applied Geophysics*, vol. 43, no. 2-4, pp. 175–187, 2000.

[7] C. W. Chang, C. H. Lin, and H. S. Lien, "Measurement radius of reinforcing steel bar in concrete using digital image GPR," *Construction and Building Materials*, vol. 23, no. 2, pp. 1057–1063, 2009.

[8] W. Al-Nuaimy, Y. Huang, M. Nakhkash, M. T. C. Fang, V. T. Nguyen, and A. Eriksen, "Automatic detection of buried utilities and solid objects with GPR using neural networks and pattern recognition," *Journal of Applied Geophysics*, vol. 43, no. 2–4, pp. 157–165, 2000.

[9] X.-Q. He, Z.-Q. Zhu, Q.-Y. Liu, and G.-Y. Lu, "Review of GPR Rebar Detection. Progress In Electromagnetics Research Symposium," in *Proceedings of the Review of GPR Rebar Detection. Progress In Electromagnetics Research Symposium*, Beijing, China, 2009.

[10] M. I. Hasan and N. Yazdani, "An experimental study for quantitative estimation of rebar corrosion in concrete using ground penetrating radar," *Journal of Engineering (United States)*, vol. 2016, 2016.

[11] S. Hong, H. Wiggenhauser, R. Helmerich, B. Dong, P. Dong, and F. Xing, "Long-term monitoring of reinforcement corrosion in concrete using ground penetrating radar," *Corrosion Science*, vol. 114, pp. 123–132, 2017.

[12] J. Hugenschmidt and R. Mastrangelo, "GPR inspection of concrete bridges," *Cement and Concrete Composites*, vol. 28, no. 4, pp. 384–392, 2006.

[13] W. Wai-Lok Lai, X. Dérobert, and P. Annan, "A review of Ground Penetrating Radar application in civil engineering: A 30-year journey from Locating and Testing to Imaging and Diagnosis," *NDT & E International*, vol. 96, pp. 58–78, 2018.

[14] C. P. F. Ulricksen, "Application of impulse radar to civil engineering," in *Application of impulse radar to civil engineering*, Lund University of Technology. Sweden: Lund, 1982.

[15] M. W. Juranty and S. B. Chase, "Ground-penetrating radar evaluation of bridge decks," in *Proceedings of the Nondestructive Evaluation of Aging Infrastructure*, pp. 59–67, Oakland, CA, USA, 2004.

[16] T. R. Cantor, "Review of penetrating radar as applied to nondestructive testing of concrete," in *ACI SP-82*, V. M. Malhotra and T. R. Cantor, Eds., vol. 20, Insituy Nondestructive Testing of Concrete, American Concrete Institute, 1984.

[17] G. G. Clemena, "Short pulse radar methods," in *Handbook on Non-destructive Testing of Concrete*, V. M. Malhotra and N. J. Carino, Eds., vol. 11, CRC Press, Boston, Mass, USA, 1991.

[18] S. Laurens, J. P. Balayssac, J. Rhazi, G. Klysz, and G. Arliguie, "Non-destructive evaluation of concrete moisture by GPR: Experimental study and direct modeling," *Materials and Structures/Materiaux et Constructions*, vol. 38, no. 283, pp. 827–832, 2005.

[19] C. Maierhofer and S. Leipold, "Radar investigation of masonry structures," *NDT & E International*, vol. 34, no. 2, pp. 139–147, 2001.

[20] J. H. Bungey, "Sub-surface radar testing of concrete: A review," *Construction and Building Materials*, vol. 18, no. 1, pp. 1–8, 2004.

[21] V. Barrile and R. Pucinotti, "Application of radar technology to reinforced concrete structures: A case study," *NDT & E International*, vol. 38, no. 7, pp. 596–604, 2005.

[22] A. V. Varnavina, L. H. Sneed, A. K. Khamzin, E. V. Torgashov, and N. L. Anderson, "An attempt to describe a relationship between concrete deterioration quantities and bridge deck condition assessment techniques," *Journal of Applied Geophysics*, vol. 142, pp. 38–48, 2017.

[23] P. Wiwatrojanagul, R. Sahamitmongkol, S. Tangtermsirikul, and N. Khamsemanan, "A new method to determine locations of rebars and estimate cover thickness of RC structures using GPR data," *Construction and Building Materials*, vol. 140, pp. 257–273, 2017.

[24] A. V. Varnavina, A. K. Khamzin, L. H. Sneed et al., "Concrete bridge deck assessment: Relationship between GPR data and concrete removal depth measurements collected after hydrodemolition," *Construction and Building Materials*, vol. 99, pp. 26–38, 2015.

[25] S. Yehia, N. Qaddoumi, S. Farrag, and L. Hamzeh, "Investigation of concrete mix variations and environmental conditions on defect detection ability using GPR," *NDT & E International*, vol. 65, pp. 35–46, 2014.

[26] M. Torres-Luque, E. Bastidas-Arteaga, F. Schoefs, M. Sánchez-Silva, and J. F. Osma, "Non-destructive methods for measuring chloride ingress into concrete: State-of-the-art and future challenges," *Construction and Building Materials*, vol. 68, pp. 68–81, 2014.

[27] X. Dérobert, J. F. Lataste, J.-P. Balayssac, and S. Laurens, "Evaluation of chloride contamination in concrete using electromagnetic non-destructive testing methods," *NDT & E International*, vol. 89, pp. 19–29, 2017.

[28] A. Zaki, S. Kabir, B. H. Abu Bakar, M. A. Megat Johari, and Y. Jusman, "Application of Image Processing for Detection of Corrosion Using Ground Penetrating Radar," in *Proceedings of the The 6th International Conference on Information Communication Technology and Systems*, Surabaya, 2010.

[29] A. Zaki and S. Kabir, "Radar-based quantification of corrosion damage in concrete structures," in *Proceedings of the Progress in Electromagnetics Research Symposium, PIERS 2011 Marrakesh*, pp. 794–798, Morocco, March 2011.

[30] S. Kabir and A. Zaki, "Detection and quantification of corrosion damage using ground penetrating radar (GPR)," in *Proceedings of the Progress in Electromagnetics Research Symposium, PIERS 2011 Marrakesh*, pp. 790–793, Morocco, March 2011.

[31] S. N. A. Mohd Kanafiah, N. D. M. Kamal, A. Z. Ahmad Firdaus et al., "Recognition system of Underground Object Shape using ground penetrating radar datagram," in *Proceedings of the 5th IEEE International Conference on Control System, Computing and Engineering, ICCSCE 2015*, pp. 488–491, Malaysia, November 2015.

[32] A. Robert, "Dielectric permittivity of concrete between 50 Mhz and 1 GHz and GPR measurements for building materials evaluation," *Journal of Applied Geophysics*, vol. 40, no. 1-3, pp. 89–94, 1998.

[33] M. N. Soutsos, J. H. Bungey, S. G. Millard, M. R. Shaw, and A. Patterson, "Dielectric properties of concrete and their influence

on radar testing," *NDT & E International*, vol. 34, no. 6, pp. 419–425, 2001.

[34] Z. M. Sbartaï, S. Laurens, J.-P. Balayssac, G. Ballivy, and G. Arliguie, "Effect of concrete moisture on radar signal amplitude," *ACI Materials Journal*, vol. 103, no. 6, pp. 419–426, 2006.

[35] C. Maierhofer, "Nondestructive evaluation of concrete infrastructure with ground penetrating radar," *Journal of Materials in Civil Engineering*, vol. 15, no. 3, pp. 287–297, 2003.

[36] U. B. Halabe, *Condition Assessment of Reinforced Concrete Structures Using Electromagnetic Waves*, Massachusetts Institute of Technology, Massachusetts, Mass, USA, 1990.

[37] A. Taffe and C. Maierhofer, "Guidelines for NDT methods in civil engineering," in *Proceedings of the The International Symposium on Non-Destructive Testing in Civil Engineering, NDT-CE*, Berlin, Germany, 2003.

[38] X. He, Z. Zhu, G. Lu, and Q. Lu, "Bridge management with GPR," in *Proceedings of the 2009 International Conference on Information Management, Innovation Management and Industrial Engineering, ICIII 2009*, pp. 329–332, China, December 2009.

[39] S. Ahmad, "Techniques for inducing accelerated corrosion of steel in concrete," *Arabian Journal for Science and Engineering*, vol. 34, no. 2 C, pp. 95–104, 2009.

[40] A. A. Almusallam, "Effect of degree of corrosion on the properties of reinforcing steel bars," *Construction and Building Materials*, vol. 15, no. 8, pp. 361–368, 2001.

[41] C. Fang, K. Lundgren, L. Chen, and C. Zhu, "Corrosion influence on bond in reinforced concrete," *Cement and Concrete Research*, vol. 34, no. 11, pp. 2159–2167, 2004.

[42] A. H. Al-Saidy, A. S. Al-Harthy, K. S. Al-Jabri, M. Abdul-Halim, and N. M. Al-Shidi, "Structural performance of corroded RC beams repaired with CFRP sheets," *Composite Structures*, vol. 92, no. 8, pp. 1931–1938, 2010.

[43] A. Zaki, H. K. Chai, A. Behnia, D. G. Aggelis, J. Y. Tan, and Z. Ibrahim, "Monitoring fracture of steel corroded reinforced concrete members under flexure by acoustic emission technique," *Construction and Building Materials*, vol. 136, pp. 609–618, 2017.

[44] K. Sakr, "Effect of cement type on the corrosion of reinforcing steel bars exposed to acidic media using electrochemical techniques," *Cement and Concrete Research*, vol. 35, no. 9, pp. 1820–1826, 2005.

[45] Y. Yuan, Y. Ji, and S. P. Shah, "Comparison of two accelerated corrosion techniques for concrete structures," *ACI Structural Journal*, vol. 104, no. 3, pp. 344–347, 2007.

[46] G. Nounu and Z.-U. Chaudhary, "Reinforced concrete repairs in beams," *Construction and Building Materials*, vol. 13, no. 4, pp. 195–212, 1999.

[47] A. A. Almusallam, A. S. Al-Gahtani, and A. R. Aziz, "Effect of reinforcement corrosion on bond strength," *Construction and Building Materials*, vol. 10, no. 2, pp. 123–129, 1996.

[48] ASTM, *G1-Standard Practice for Preparing, Cleaning, and Evaluating Corrosion Test Specimens*, 2003.

[49] ASTM, *G3 -72-Standard Practice for Laboratory Immersion Corrosion Testing of Metals*, 2004.

[50] T. A. El Maaddawy and K. A. Soudki, "Effectiveness of impressed current technique to simulate corrosion of steel reinforcement in concrete," *Journal of Materials in Civil Engineering*, vol. 15, no. 1, pp. 41–47, 2003.

[51] C. A. Apostolopoulos and D. Michalopoulos, "Impact of corrosion on mass loss, fatigue and hardness of BSt500 s steel," *Journal of Materials Engineering and Performance*, vol. 16, no. 1, pp. 63–67, 2007.

[52] C. A. Apostolopoulos, D. Michalopoulos, and P. Koutsoukos, "The corrosion effects on the structural integrity of reinforcing steel," *Journal of Materials Engineering and Performance*, vol. 17, no. 4, pp. 506–516, 2008.

[53] G. Klysz, J.-P. Balayssac, and S. Laurens, "Spectral analysis of radar surface waves for non-destructive evaluation of cover concrete," *NDT & E International*, vol. 37, no. 3, pp. 221–227, 2004.

[54] W. L. Lai, S. C. Kou, W. F. Tsang, and C. S. Poon, "Characterization of concrete properties from dielectric properties using ground penetrating radar," *Cement and Concrete Research*, vol. 39, no. 8, pp. 687–695, 2009.

[55] C. L. Barnes, J.-F. Trottier, and D. Forgeron, "Improved concrete bridge deck evaluation using GPR by accounting for signal depth-amplitude effects," *NDT & E International*, vol. 41, no. 6, pp. 427–433, 2008.

[56] W.-L. Lai, T. Kind, M. Stoppel, and H. Wiggenhauser, "Measurement of accelerated steel corrosion in concrete using ground-penetrating radar and a modified half-cell potential method," *Journal of Infrastructure Systems*, vol. 19, no. 2, pp. 205–220, 2013.

[57] C. Maierhofer and A. Taffe, "Guidelines for NDT methods in civil engineering," in *Nondestructive Testing in Civil Engineering (NDTCE)*, Berlin, Germany, 2003.

[58] W. L. Lai, T. Kind, and H. Wiggenhauser, "Detection of accelerated reinforcement corrosion in concrete by ground penetrating radar," in *Proceedings of the 13th Internarional Conference on Ground Penetrating Radar, GPR 2010*, Italy, June 2010.

[59] R. W. Arndt, J. Cui, D. R. Huston, D. O. Thompson, and D. E. Chimenti, "Monitoring of reinforced concrete corrosion and deterioration by periodic multi-sensor non-destructive evaluation," in *Proceedings of 37th Annual Review of Progress in Quantitative Nondestructive Evaluation, QNDE 2010*, vol. 20A, pp. 1371–1378, San Diego, Ca, USA.